Tailoring Plasmon Coupling in Self-Assembled One-Dimensional Au Nanoparticle Chains through Simultaneous Control of Size and Gap Separation

ARTICLE *in* JOURNAL OF PHYSICAL CHEMISTRY LETTERS · JUNE 2013

Impact Factor: 7.46 · DOI: 10.1021/jz401066g · Source: PubMed

5 AUTHORS, INCLUDING:

Amin Feizpour
Boston University
12 PUBLICATIONS **49** CITATIONS

SEE PROFILE

THE JOURNAL OF PHYSICAL CHEMISTRY Letters

Letter

pubs.acs.org/JPCL

Tailoring Plasmon Coupling in Self-Assembled One-Dimensional Au Nanoparticle Chains through Simultaneous Control of Size and Gap Separation

Tianhong Chen, Mahshid Pourmand, Amin Feizpour, Bradford Cushman, and Björn M. Reinhard*

Department of Chemistry and the Photonics Center, Boston University, Boston, Massachusetts 02215, United States

Supporting Information

ABSTRACT: We investigated the near- and far-field response of 1D chains of Au nanoparticles (NPs) fabricated with high structural control through template guided self-assembly. We demonstrate that the density of poly(ethylene glycol) ligands grafted onto the NP surface, in combination with the buffer conditions, facilitate a systematic variation of the average gap width (g) at short separations of g < 1.1 nm. The overall size (n) of the individual clusters was controlled through the template. The ability to independently vary n and g allowed for a rational tuning of the spectral response in individual NP clusters over a broad spectral range. We used this structural control for a systematic investigation of the electromagnetic coupling underlying the superradiant cluster mode. Independent of the chain length, plasmon coupling is dominated by direct neighbor interactions. A decrease in coupling strength at separations $\lesssim$0.5 nm indicates the presence of nonlocal or quantum-mechanical coupling mechanisms.

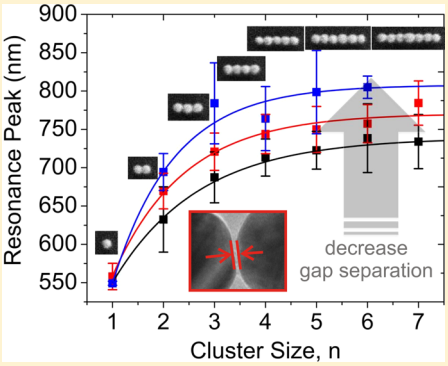

SECTION: Plasmonics, Optical Materials, and Hard Matter

Noble-metal nanoparticles (NPs) with sizes of ~50 nm and below represent – in a first approximation – dipole antennas,[1,2] in which a resonant excitation of coherent collective electron oscillations leads to large amplitude charge density oscillations referred to as localized surface plasmons (LSPs).[3] LSPs concentrate incident electromagnetic radiation in the evanescent field surrounding the NPs by many orders of magnitude and can efficiently absorb and reradiate resonant electromagnetic radiation. Although the optical properties of individual noble-metal NPs are already impressive, one of the fascinating properties of plasmonic NPs is that the assembly of NPs into "plasmonic molecules" or larger assemblies can further enhance these properties or create entirely new properties.[4−11] The exact near- and far-field properties of an individual plasmonic molecule depend not only on the interparticle separation[12−18] but also on its size[5] and geometry.[19,20] Because of their high symmetry, 1D NP clusters (or chains) are important model systems for elucidating the short- and long-range coupling mechanisms in NP clusters.[21−23] Additional interest in these nanostructures stems from the fact that propagating surface plasmon polaritons (SPPs) can be launched into these nanostructures, creating a directed energy transfer along the chain.[24,25] The interparticle separation plays a crucial role for the transfer efficiency along the chain, and it was shown that a minimization of gap width (g) facilitates a reduction of radiative losses due to efficient excitation of subradiant collective modes.[25] Similarly, the intriguing effect of cascaded field enhancement in resonant NP clusters requires short interparticle separations.[26,27]

Although NP chains have been intensely studied by several groups[21−23,25,28−33] for almost two decades, the full potential of these materials is still yet to be realized. One significant challenge in the field is that even with state-of-the-art nanofabrication techniques it remains hard to vary g in the range of strong electromagnetic coupling in a rational fashion. With electron beam lithography (EBL), for instance, which has a resolution limit of ~5 nm, it is very difficult to realize gap separations below 10 nm reliably. We overcome this fabrication challenge by assembling poly(ethylene glycol) (PEG)-functionalized NPs into lithographically defined assembly sites, which pattern the formation of closely packed 1D NP clusters. The average g in the clusters depends on the PEG ligand density and buffer conditions, and we used this approach to systematically characterize the interplay between g and cluster size (n) in determining the collective electromagnetic response in the regime of electromagnetic strong coupling.

Mapping the Influence of Gap Width and Cluster Size on the Optical Response through Generalized Multiple Particle Mie Theory (GMT) Simulations. In a first step, we applied GMT simulations to profile the near- and far-field response of 1D 40 nm (diameter) gold NP clusters of defined size as a function of gap width in the range of g = 1−5 nm. We limited the minimum separation to 1 nm in these calculations because classical electrodynamic GMT simulations cannot be reliably

Received: May 23, 2013
Accepted: June 13, 2013
Published: June 13, 2013

   dx.doi.org/10.1021/jz401066g | J. Phys. Chem. Lett. 2013, 4, 2147−2152

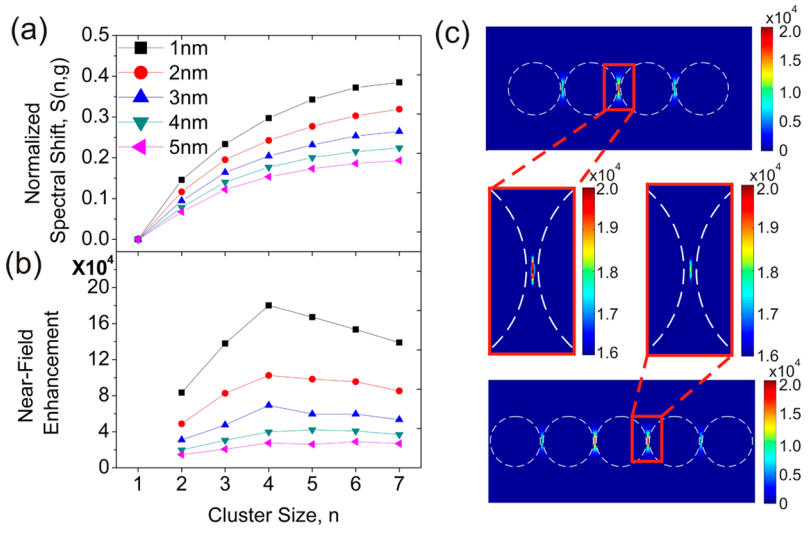

Figure 1. GMT-simulated normalized spectral shift S (a) and peak near-field intensity enhancement ($|E|^2/|E_0|^2$) (b) as function of cluster size (n) and interparticle separation (g). (c) Near-field intensity enhancement maps calculated at the wavelength of peak enhancement for n = 4 (top) and n = 5 (bottom). Insets show enlargements of the hottest-spots in the two clusters with rescaled ($|E|^2/|E_0|^2$) color map.

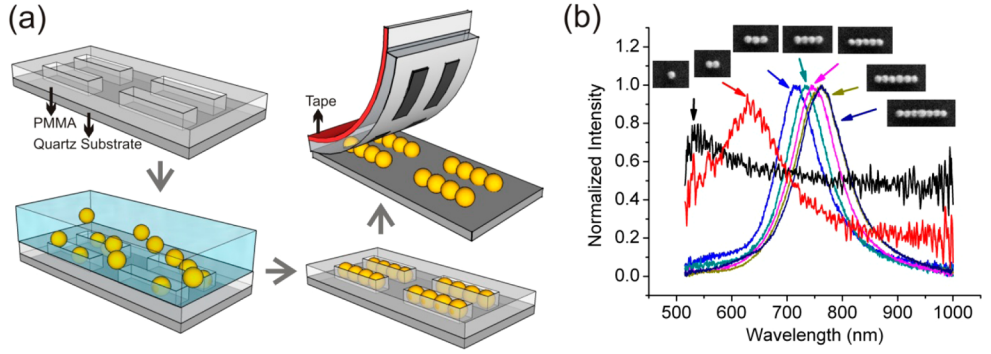

Figure 2. (a) Schematic flowchart of the template guided self-assemble approach used for fabricating 1D NP clusters. (b) Scattering spectra and corresponding SEM images of 1D clusters of various sizes; monomer (black) and dimer (red) spectra are smoothed by a nine-point sliding average.

used for shorter separations due to increasing importance of nonlocal and quantum effects at very short separations.[34−36] In Figure 1a we plot the normalized spectral shift calculated from simulated scattering cross sections as:

$$S(n, g) = \frac{\lambda_{n,g} - \lambda_0}{\lambda_0} = \Delta\lambda(n, g)/\lambda_0 \quad (1)$$

,where $\lambda_{n,g}$ is the fitted peak wavelength for a cluster as function of n and g and λ_0 is the resonance wavelength of the noninteracting individual 40 nm gold NPs. The LSPR red shifts with decreasing g and increasing n, but the change in $S(n,g)$ calculated between n+1 and n decreases with growing n in the investigated size range n = 2−7. This convergence in the spectral shift is consistent with previous observations in 2D NP clusters[5,19,37] as well as with previous studies[38] on NP chains and can be easily rationalized by the fact that plasmon coupling is a nearest-neighbor interaction. The latter also has pronounced effects on the near-field response as a function of n. In Figure 1b we plot the calculated peak near-field intensity enhancements, $|E|^2/|E_0|^2$, as function of n and g. E-field intensity enhancements were evaluated at the midpoint of the central cluster gaps, where the enhancements were highest. $|E|^2/|E_0|^2$ shows a local maximum at n = 4 in strongly coupled NP chains with short separations, g < 3 nm. This maximum is intuitively understood as compensation of two size-dependent effects. Plasmon coupling along the chain enhances the net dipole field along the chain axis and thus amplifies the coupling between the individual NP in the cluster, but it also increases the mode volume of the hybridized mode with growing n. Consequently, the delocalization of the field results in a slight net decrease in peak E-field intensity in 1D NP clusters with n > 4. This is illustrated in Figure 1c, where we compare the E-field intensity maps for the superradiant resonance modes (effective dipole fields in all NPs are aligned) of n = 4 and 5. We emphasize, however, that the relative difference in peak E-field intensity is modest and that the E-field intensity enhancement remains high for larger cluster sizes.

The performed numerical simulations, which are in qualitative agreement with recent analytical analyses of similar plasmonic systems,[11,39,40] confirm a sensitive dependence of $\Delta\lambda$ and $|E|^2$ on both n and g in the range of classical strong electromagnetic coupling. Fabrication approaches are required that provide control of n and g, ideally, in clusters with interparticle separations below the EBL limit of ∼5 nm to take full advantage of this tunability in real plasmonic materials

Template Guided Assembly of 1D Clusters. Our strategy for creating clusters of strongly coupled NPs at predefined locations is outlined in Figure 2a. EBL is not used to directly write the plasmonic structure but to create a mask, which

dx.doi.org/10.1021/jz401066g | J. Phys. Chem. Lett. 2013, 4, 2147−2152

defines locations for the subsequent self-assembly of PEG-functionalized NPs. The size and shape of the assembly site determines the NP cluster configuration obtained in this process.[19] The PEG ligands grafted to the NP surface play a dual role in this strategy because they stabilize and direct the NPs in an electrostatically guided self-assembly[37] approach and, at the same time, act as spacers between close-packed NPs on the assembly sites. We used in this work relatively short thiolated PEGs of the form HS-$(CH_2)_{11}$-$(EG)_6$-OCH_2−COOH as spacers because they assemble into a dense brush on the surface of gold NPs. We used two control parameters to tune the NP separation in the assembled chains. We varied the brush thickness by controlling the PEG surface concentration, and we varied the Debye screening length through choice of the electrolyte concentration in the buffer used during the assembly. NPs with two different PEG surface concentrations were obtained by incubating 40 nm (nominal diameter) citrate-stabilized NPs with an aqueous solution of PEGs in the molar ratios NP/PEG $1{:}5 \times 10^7$ and $1{:}5 \times 10^6$ for 24 h. We refer to these two NPs as NP_{HC} and NP_{LC} in the following. The hydrodynamic radii of these particles were 37 nm (NP_{HC}, PDI = 0.236) versus 33 nm (NP_{LC}, PDI = 0.248) in T100 (100 mM NaCl, 10 mM Tris·HCl, pH 8) and T40 (40 mM NaCl, 10 mM Tris·HCl, pH 8). The average zeta potentials were $\zeta = -45$ and −42 mV for NP_{HC} in T40 and T100, respectively. For the NP_{LC} in T100, we measured $\zeta = -24$ mV. Because of their negative surface charge in pH 8, the NPs assembled efficiently into the polylysine-treated (and thus positively charged) trenches generated by EBL in a PMMA film. The length of the trenches was varied between 90 and 500 nm to pattern different cluster sizes. SEM images of assembled 1D NP clusters are shown in Figure 2b. We found that the NPs were preferentially organized into clusters with very close particle contacts. We ascribe this clustering to a self-focusing effect due to capillary forces in the trenches.[41,42]

Size and Gap Width Dependence of the Far-Field Scattering Spectra. The spectral position of the superradiant mode in a chain of NPs depends on both n and g. For clusters of known size, elastic scattering spectroscopy is a uniquely useful tool for quantifying systematic differences in g in clusters assembled from NPs with different surface ligand concentrations or buffer salt concentrations. We hypothesized that it was possible to modulate the intracluster coupling through the PEG brush density on the NPs and the screening length (δ_D) of the buffer. Increasing brush density and δ_D is anticipated to lead to higher interparticle repulsion and thus larger interparticle separations during the NP assembly. To test this hypothesis, we monitored the peak plasmon resonance wavelength in clusters assembled from NP_{HC} and NP_{LC} in T100 (δ_D = 1.52 nm) and from NP_{HC} in T40 (δ_D = 0.96 nm).

We recorded the scattering spectra of individual NP clusters under oblique white-light illumination in a conventional dark-field microscope. Before the scattering spectra were recorded, each individual cluster was first inspected under the scanning electron microscope (SEM) to determine its morphology and cluster size n. The acceleration voltage of SEM in these experiments was chosen to be sufficiently low (1.5 keV) to avoid any structural modifications of the NP clusters that could affect their light scattering properties. As expected for these strongly anisotropic clusters, the resonance wavelength of the longitudinal mode is strongly red-shifted relative to the vertical mode (Figure S1 in the Supporting Information). Consistent with the performed simulations, we observe that the magnitude of this red shift increases with n for clusters generated under identical assembly conditions (Figure 2).

Figure 3a summarizes the experimentally determined normalized spectral shift S for NP clusters in the size range n

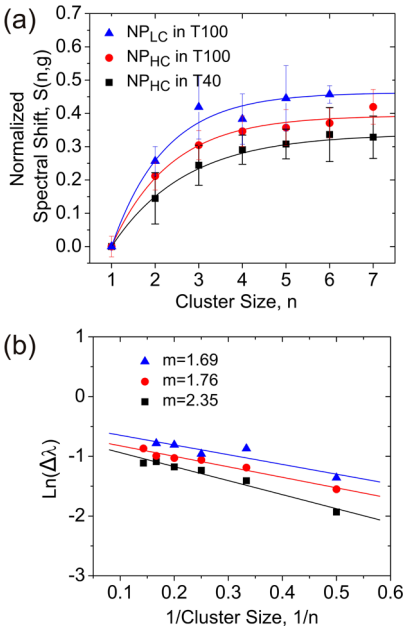

Figure 3. (a) Experimental normalized spectral shift S as function of cluster size (n) and interparticle separation (g). (b) Natural log of the peak shift ratio versus the inverse of cluster size ($1/n$).

= 1−7. All of the experimental S relationships show initial red shifts with increasing n for small cluster sizes that converge at $n \approx 4$, as predicted by the GMT simulations. The S relationships obtained for the three different experimental conditions differ, however, in their slopes and the asymptotic saturation values S_{max}. The slopes and S_{max} values vary with changes in PEG brush density and ionic screening in the following order: (NP_{HC}; T40) < (NP_{HC}; T100) < (NP_{LC}; T100). This finding confirms that PEG ligand density and ionic strength allow for a systematic variation of the plasmon coupling in the chain.

To verify that the observed spectral differences for the different experimental conditions indeed arose from systematic differences in the interparticle separation, we took advantage of the flexibility of the template guided self-assembly that allows patterning of NP clusters on a wide range of substrates and fabricated NP chains on Si_3N_4 membranes (see Methods), which are transparent for the electron beam. The latter facilitates a systematic characterization of the interparticle separations in 1D NP clusters through high-resolution transmission electron microscopy (HRTEM) (Figure 4a). We determined the interparticle separations in nontouching gap structures from the TEM images. We fitted the raw data with a Gaussian function, in which three standard deviations comprised 99.7% of the data to remove outliers. The resulting distributions are plotted as cumulative probability plots in Figure 4b. Consistent shifts between the plots confirm that the observed spectral shifts in Figure 3a are correlated with systematic increases in the interparticle separations. The average interparticle separation (cumulative probability of 0.5) increases for the clusters fabricated on Si_3N_4 membranes from g = 0.37 nm in the case of (NP_{LC}; T100) over 0.53 nm for (NP_{HC}; T100) to g = 1.08 nm for (NP_{HC}; T40). We also

dx.doi.org/10.1021/jz401066g | J. Phys. Chem. Lett. 2013, 4, 2147−2152

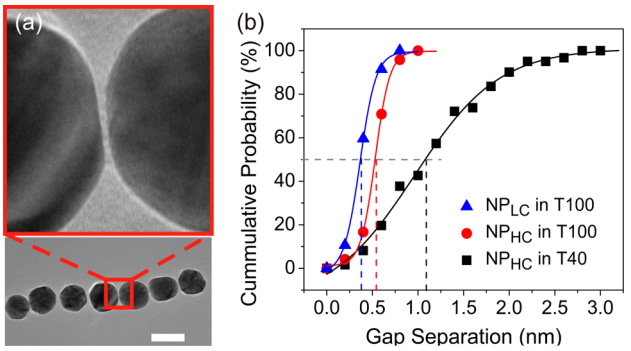

Figure 4. (a) HRTEM pictures of 1D clusters formed from NP_{NC} in T40 buffer; scale bar represents 50 nm. (b) Cumulative probability plots for the interparticle gap distributions obtained under three different experimental conditions as defined in the legend.

performed Student's t tests for the distributions in Figure 4b and found that differences between the distributions were highly significant ($p < 1.76 \times 10^{-4}$).

The spectral shift, $\Delta\lambda$, obtained for the different experimental conditions is found to be well-described (Figure 3b) by a function of the form[21,43]

$$\Delta\lambda = \lambda_0 e^{-m/n} \quad (2)$$

Harris et al.[21] introduced m as a characteristic length, defined in units of chain periods, of electromagnetic coupling in a plasmonic NP chain. The experimental m values for the clusters investigated in this work lie in the range of 1.6 to 2.3 and thus confirm that electromagnetic next-neighbor interactions dominate the plasmon coupling in the chain. A strong localization of the electromagnetic interactions in the chain is in excellent agreement with the previous theoretical investigations, which predicted $m \approx 2.0$ in the relevant g range.[21] In our experimental studies we find that m systematically decreases with decreasing g. The average interparticle separations for (NP_{LC}; T100) and (NP_{HC}; T100) are already close to the separation range, where nonlocal[34] or quantum plasmonic effects[35,44] have been shown to be relevant for Au NP dimers. The measured decrease in m is consistent with a reduced interparticle coupling in the NP chain due to non-negligible contributions from nonclassic electromagnetic coupling at the short separations accessible with the chosen PEG spacer.

In conclusion, we have demonstrated that ligand density and buffer conditions are important control parameters in the template guided self-assembly of plasmonic NP clusters that facilitate a systematic variation of g on very short length scales. We applied this approach to tailor plasmon coupling in 1D NP clusters. We shifted the far-field resonance of the superradiant mode in NP chains by up to 250 nm through variation of n between $n = 1$ and 7 (at constant g) and up to 100 nm through variation of g between 0.37 nm and 1.08 nm (at constant n). A characterization of the spectral shift as a function of g confirmed a preferential localization of the electromagnetic interactions between neighboring NPs and indicated significant contribution from nonclassical coupling mechanisms for $g \lesssim 0.5$ nm.

EXPERIMENTAL METHODS

GMT Simulations. The simulations were performed with the open source-code MSTM 2.2.[45] The maximum multipolar order in the series expansion of the vector spherical harmonics was determined by the default convergence criterion. The size of the particles was assumed to be 20 nm in radius, and g was identical for all gaps of one cluster. For the far-field simulations, we assumed an incident angle of 48° to take into account the numerical aperture of the microscope. The spectra were averaged over two polarizations (along and perpendicular to the long dimer axis). In the near-field simulations the polarization of the incident light pointed along the long cluster axis. All simulations were performed with a refractive index of $n_r = 1.5$.

Particle Preparation. 1 mL of commercial citrate-stabilized 40 nm Au particles in aqueous solution (British Biocell International) was mixed with 5 μL of 1% or 0.1% (v/v) HS-$C_{11}H_{22}$-EG_6-COOH (PEG, EG=OCH_2CH_2) and incubated 24 h to obtain PEG-functionalized particles NP_{HC} and NP_{LC}, respectively. The particles were cleaned by centrifugation and resuspended in a 10 mM Tris·HCl buffer (pH 8.0) containing 40 or 100 mM NaCl. Hydrodynamic radii of NPs were measured using a Malvern NANO-ZS90 Zetasizer at 25 °C.

Self-Assembly of 1D Clusters. A layer of poly(methyl methacrylate) (PMMA) was spin-coated on a quartz substrate and then patterned with a Zeiss SUPRA 40VP SEM equipped with Raith beam blanker and a nanopattern generation system (NPGS). 40 nm wide trenches of different length (90 nm-500 nm) were generated. The patterned quartz substrates with PMMA mask were incubated with a 2% (w/w) poly lysine solution for 2 h and then washed with water. A drop of the concentrated Au particle solution (7nM) was placed on top of the patterned trenches and moved across the surface along the direction of trenches 50 times with an air stream. The remaining NP solution was then washed away with water. After the samples were dried, the PMMA layer was stripped off the substrate using double-sided tape (UltraTape #1510).

Dark-Field Scattering Characterization of NP Clusters. Scattering spectra were taken with an upright microscope (Olympus BX51 WI). The samples were illuminated through an oil dark-field condenser (NA 1.2 to 1.4). The signal was collected with a 60× air objective lens (Olympus LUCPLFLN, NA 0.7) and spectra were recorded by a spectrometer (Andor SR303i) equipped with a CCD camera (Andor DU401-BR-DD). Spectra were background-corrected and normalized by the excitation profile of the white light source (100W tungsten halogen lamp). Multiple clusters in one binding site led to separated spectral peaks and were omitted from analysis. All spectra were acquired in air.

TEM Sample Preparation. TEM grid with 20 nm Si_3N_4 membrane (SPI Supplies/Structure Probe) was spin-coated with a layer of PMMA and patterned with the same procedure as described above. Approximately 100 clusters were evaluated for each condition on a JEOL JEM 2010 HRTEM with 200 kV HT and 100k× magnification. Not all gaps were resolvable in 2D TEM images; unresolvable gaps were not included in the data analysis.

ASSOCIATED CONTENT

Supporting Information

Polarization dependent scattering spectra of representative 1D nanoparticle cluster. This material is available free of charge via the Internet at http://pubs.acs.org.

AUTHOR INFORMATION

Corresponding Author

*E-mail: bmr@bu.edu.

Author Contributions

The manuscript was written through contributions of all authors.

Notes

The authors declare no competing financial interest.

■ ACKNOWLEDGMENTS

This work was supported by the National Science Foundation through grants 1159552, 0853798, and 0953121 and by the National Institutes of Health (NIH/NCI) through grant 5R01CA138509.

■ REFERENCES

(1) Halas, N. J. Connecting the Dots: Reinventing Optics for Nanoscale Dimensions. *Proc. Natl. Acad. Sci. U. S. A.* **2009**, *106*, 3643.
(2) Kelly, K. L.; Coronado, E.; Zhao, L. L.; Schatz, G. C. The Optical Properties of Metal Nanoparticles: The Influence of Size, Shape, And Dielectric Environment. *J. Phys. Chem. B* **2003**, *107*, 668.
(3) Halas, N. J.; Lal, S.; Chang, W. S.; Link, S.; Nordlander, P. Plasmons in Strongly Coupled Metallic Nanostructures. *Chem. Rev. (Washington, DC, U. S.)* **2011**, *111*, 3913.
(4) Fraire, J. C.; Perez, L. A.; Coronado, E. A. Rational Design of Plasmonic Nanostructures for Biomolecular Detection: Interplay between Theory and Experiments. *ACS Nano* **2012**, *6*, 3441.
(5) Yan, B.; Boriskina, S. V.; Reinhard, B. M. Design and Implementation of Noble Metal Nanoparticle Cluster Arrays for Plasmon Enhanced Biosensing. *J. Phys. Chem. C* **2011**, *115*, 24437.
(6) Li, K. R.; Stockman, M. I.; Bergman, D. J. Self-Similar Chain of Metal Nanospheres As an Efficient Nanolens. *Phys. Rev. Lett.* **2003**, *91*, 227402.
(7) Ahn, W.; Boriskina, S. V.; Hong, Y.; Reinhard, B. M. Electromagnetic Field Enhancement and Spectrum Shaping in Plasmonically Integrated Optical Vortices. *Nano Lett.* **2012**, *12*, 219.
(8) Boriskina, S. V.; Reinhard, B. M. Molding the Flow of Light on the Nanoscale from Vortex Nanogears to Phase-Operated Plasmonic Machinery. *Nanoscale* **2012**, *4*, 76.
(9) Fan, J. A.; Wu, C.; Bao, K.; Bao, J.; Bardhan, R.; Halas, N. J.; Manoharan, V.; Nordlander, P.; Shvets, G.; Capasso, F. Self-Assembled Plasmonic Nanoparticle Clusters. *Science* **2010**, *328*, 1135.
(10) Wang, H.; Brandl, D. W.; Nordlander, P.; Halas, N. J. Plasmonic Nanostructures: Artificial Molecules. *Acc. Chem. Res.* **2007**, *40*, 53.
(11) Sun, G.; Khurgin, J. B. Comparative Study of Field Enhancement between Isolated and Coupled Metal Nanoparticles: An Analytical Approach. *Appl. Phys. Lett.* **2010**, *97*, 263110.
(12) Jain, P. K.; El-Sayed, M. A. Surface Plasmon Coupling and Its Universal Size Scaling in Metal Nanostructures of Complex Geometry: Elongated Particle Pairs and Nanosphere Trimers. *J. Phys. Chem. C* **2008**, *112*, 4954.
(13) Yang, L.; Wang, H.; Yan, B.; Reinhard, B. M. Calibration of Silver Plasmon Rulers in the 1−25 nm Separation Range: Experimental Indications of Distinct Plasmon Coupling Regimes. *J. Phys. Chem. C* **2010**, *114*, 4901.
(14) Reinhard, B. M.; Siu, M.; Agarwal, H.; Alivisatos, A. P.; Liphardt, J. Calibration of Dynamic Molecular Rule Based on Plasmon Coupling between Gold Nanoparticles. *Nano Lett.* **2005**, *5*, 2246.
(15) Jain, P. K.; Huang, W. Y.; El-Sayed, M. A. On the Universal Scaling Behavior of the Distance Decay of Plasmon Coupling in Metal Nanoparticle Pairs: A Plasmon Ruler Equation. *Nano Lett.* **2007**, *7*, 2080.
(16) Lamprecht, B.; Schider, G.; Lechner, R. T.; Ditlbacher, H.; Krenn, J. R.; Leitner, A.; Aussenegg, F. R. Metal Nanoparticle Gratings: Influence of Dipolar Particle Interaction on the Plasmon Resonance. *Phys. Rev. Lett.* **2000**, *84*, 4721.
(17) Zou, S. L.; Schatz, G. C. Narrow Plasmonic/Photonic Extinction and Scattering Line Shapes for One and Two Dimensional Silver Nanoparticle Arrays. *J. Chem. Phys.* **2004**, *121*, 12606.
(18) Gunnarsson, L.; Bjerneld, E. J.; Xu, H.; Petronis, S.; Kasemo, B.; Kall, M. Interparticle Coupling Effects in Nanofabricated Substrates for Surface-Enhanced Raman Scattering. *Appl. Phys. Lett.* **2001**, *78*, 802.
(19) Yan, B.; Boriskina, S. V.; Reinhard, B. M. Optimizing Gold Nanoparticle Cluster Configurations ($n \leq 7$) for Array Applications. *J. Phys. Chem. C* **2011**, *115*, 4578.
(20) Jain, T.; Westerlund, F.; Johnson, E.; Moth-Poulsen, K.; Bjornholm, T. Self-Assembled Nanogaps via Seed-Mediated Growth of End-to-End Linked Gold Nanorods. *ACS Nano* **2009**, *3*, 828.
(21) Harris, N.; Arnold, M.; Blaber, M. G.; Ford, M. J. Plasmonic Resonances of Closely Coupled Gold Nanosphere Chains. *J. Phys. Chem. C* **2009**, *113*, 2784.
(22) Pinchuk, A. O.; Schatz, G. C. Nanoparticle Optical Properties: Far- And near-Field Electrodynamic Coupling in a Chain of Silver Spherical Nanoparticles. *Mater. Sci. Eng., B* **2008**, *149*, 251.
(23) Alu, A.; Engheta, N. Theory of Linear Chains of Metamaterial/Plasmonic Particles As Subdiffraction Optical Transmission Lines. *Phys. Rev. B* **2006**, *74*, 205436.
(24) Maier, S. A.; Kik, P. G.; Atwater, H. A.; Meltzer, S.; Harel, E.; Koel, B. E.; Requicha, A. A. G. Local Detection of Electromagnetic Energy Transport below the Diffraction Limit in Metal Nanoparticle Plasmon Waveguides. *Nat. Mater.* **2003**, *2*, 229.
(25) Willingham, B.; Link, S. Energy Transport in Metal Nanoparticle Chains via Sub-Radiant Plasmon Modes. *Opt. Express* **2011**, *19*, 6450.
(26) Toroghi, S.; Kik, P. G. Cascaded Field Enhancement in Plasmon Resonant Dimer Nanoantennas Compatible with Two-Dimensional Nanofabrication Methods. *Appl. Phys. Lett.* **2012**, *101*, 013116.
(27) Toroghi, S.; Kik, P. G. Cascaded Plasmon Resonant Field Enhancement in Nanoparticle Dimers in the Point Dipole Limit. *Appl. Phys. Lett.* **2012**, *100*, 183105.
(28) Arnold, M. D.; Blaber, M. G.; Ford, M. J.; Harris, N. Universal Scaling of Local Plasmons in Chains of Metal Spheres. *Opt. Express* **2010**, *18*, 7528.
(29) Fung, K. H.; Chan, T. H. Plasmonic Modes in Periodic Metal Nanoparticles Chains: A Direct Dynamic Eigenmode Analysis. *Opt. Lett.* **2007**, *32*, 973.
(30) Govyadinov, A. A.; Markel, V. A. From Slow to Supraluminal Propagation: Dispersive Properties of Surface Plasmon Polaritons in Linear Chains of Metallic Nanospheroids. *Phys. Rev. B.* **2008**, *78*, 035403.
(31) Wei, Q. H.; Su, K. H.; Durant, S.; Zhang, X. Plasmon Resonance of Finite One-Dimensional Au Nanoparticle Chains. *Nano Lett.* **2004**, *4*, 1067.
(32) Thomas, K. G.; Barazzouk, S.; Ipe, B. I.; Joseph, S. T. S.; Kamat, P. V. Uniaxial Plasmon Coupling through Longitudinal Self-Assembly of Gold Nanorods. *J. Phys. Chem. B* **2004**, *108*, 13066.
(33) Wang, Y.; DePrince, A. E., III; Gray, S. K.; Lin, X.-M.; Pelton, M. Solvent-Mediated End-to-End Assembly of Gold Nanorods. *J. Phys. Chem. Lett.* **2010**, *1*, 2692.
(34) de Abajo, F. J. G. Nonlocal Effects in the Plasmons of Strongly Interacting Nanoparticles, Dimers, And Waveguides. *J. Phys. Chem. C* **2008**, *112*, 17983.
(35) Zuluoga, J.; Prodan, E.; Nordlander, P. Quantum Description of the Plasmon Resonance of a Nanoparticle Dimer. *Nano Lett.* **2009**, *9*, 887.
(36) Marinica, D. C.; Kazansky, A. K.; Nordlander, P.; Aizpurua, J.; Borisov, A. G. Quantum Plasmonics: Nonlinear Effects in the Field Enhancement of a Plasmonic Nanoparticle Dimer. *Nano Lett.* **2012**, *12*, 1333.
(37) Yan, B.; Thubagere, A.; Premasiri, R.; Ziegler, L.; Dal Negro, L.; Reinhard, B. M. Engineered SERS Substrates with Multiscale Signal Enhancement: Nanoparticle Cluster Arrays. *ACS Nano* **2009**, *3*, 1190.
(38) Slaughter, L. S.; Willingham, B. A.; Chang, W.-S.; Chester, M. H.; Ogden, N.; Link, S. Toward Plasmonic Polymers. *Nano Lett.* **2012**, *12*, 3967.

(39) Sun, G.; Khurgin, J. B.; Soref, R. A. Plasmonic Light-Emission Enhancement with Isolated Metal Nanoparticles and Their Coupled Arrays. *J. Opt. Soc. Am. B* **2008**, *25*, 1748.
(40) Khurgin, J. B.; Sun, G.; Soref, R. A. Practical Limits of Absorption Enhancement near Metal Nanoparticles. *Appl. Phys. Lett.* **2009**, *94*, 071103.
(41) Fustin, C. A.; Glasser, G.; Spiess, H. W.; Jonas, U. Parameters Influencing the Templated Growth of Colloidal Crystals on Chemically Patterned Surfaces. *Langmuir* **2004**, *20*, 9114.
(42) Kralchevsky, P. A.; Nagayama, K. Capillary Forces Between Colloidal Particles. *Langmuir* **1994**, *10*, 23.
(43) Abargues, R.; Albert, S.; Valdes, J. L.; Abderrafi, K.; Martinez-Pastor, J. P. Molecular-Mediated Assembly of Silver Nanoparticles with Controlled Interparticle Spacing and Chain Length. *J. Mater. Chem.* **2012**, *22*, 22204.
(44) Scholl, J. A.; Garcia-Etxarri, A.; Koh, A. L.; Dionne, J. A. Observation of Quantum Tunneling between Two Plasmonic Nanoparticles. *Nano Lett.* **2012**, *13*, 564.
(45) Mackowski, D. W.; Mishchenko, M. I. Calculation of the T Matrix and the Scattering Matrix for Ensembles of Spheres. *J. Opt. Soc. Am. A* **1996**, *13*, 2266.